HHS Public Access

Author manuscript

J Vestib Res. Author manuscript; available in PMC 2022 April 08.

Published in final edited form as:

J Vestib Res. 2021 ; 31(6): 441–449. doi:10.3233/VES-201591.

Functional cooperation between two otoconial proteins Oc90 and Nox3

Yinfang Xu[1], **Liping Yang**[1,3], **Xing Zhao**[1], **Yan Zhang**[1], **Timothy A. Jones**[2], **Sherri M. Jones**[2], **Yunxia Wang Lundberg**[1,#]

[1]Vestibular Genetics Laboratory, Boys Town National Research Hospital, Omaha, NE 68131, USA

[2]Department of Special Education and Communication Disorders, University of Nebraska-Lincoln, Lincoln, NE 68583, USA

[3]Current address: Changsha Environmental Protection College, 10 Jinggui Rd, Yuhua Qu, Changsha, Hunan, China

Abstract

BACKGROUND: Otoconia-related vertigo and balance deficits are common in humans, but the molecular etiology is unknown at present.

OBJECTIVE: In order to study mechanisms of otoconia formation and maintenance, we have investigated whether otoconin-90 (Oc90), the predominant otoconial constituent protein, and the NADPH oxidase Nox3, an essential regulatory protein for otoconia formation, are functionally interlinked.

METHODS: We performed balance behavioral, electrophysiological, morphological and molecular cellular analyses.

RESULTS: Double heterozygous mutant mice for *Oc90* and *Nox3* show severe imbalance, albeit less profound than double null mutants. In contrast, single heterozygous mutant mice have normal balance. Double heterozygous mice have otoconia defects and double null mice have no otoconia. In addition, some hair bundles in the latter mice go through accelerated degeneration. *In vitro* calcification analysis in cells stably expressing these proteins singly and doubly shows much more intense calcification in the double transfectants.

CONCLUSIONS: Oc90 and Nox3 augment each other's function, which is not only critical for otoconia formation but also for hair bundle maintenance.

Keywords

Oc90; Nox3; calcification; hair bundle; balance

[#]**Corresponding author:** Yunxia (Yesha) Wang Lundberg, Ph.D., Director, Vestibular Genetics Laboratory, Boys Town National Research Hospital, 555 N. 30th St., Omaha, NE 68131, Ph. 1-531-355-6735, Fax: 1-531-355-6351, Yesha.Lundberg@boystown.org.

Conflict of interest

The authors declare no conflict of interest.

Introduction

Otoconia are bio-crystals of $CaCO_3$ and proteins overlaying the macular sensory epithelium of the utricle and saccule in the vertebrate inner ear. These crystals are critical for the macula to detect gravity and linear head motion, and therefore for the individual/animal to maintain bodily balance. Abnormal size, shape or organization of otoconia, as well as the dislocation of those minute crystals, can affect motion-sensing and lead to vertigo and imbalance [1, 6, 11, 18, 27]. Over the last two decades, efforts have been made to unravel the molecular mechanisms responsible for otoconia formation, maintenance and anchoring. To date, over 24 mouse and 75 zebrafish otoconia-related genes have been identified [15]. About half of them encode otoconial constituent or anchoring proteins, while the other half are responsible for regulating otoconia formation. In order for otoconia to properly form, expression of these genes must be tightly regulated spatiotemporally [25]. In addition, evidence suggests a high degree of coordination among different otoconial component proteins in the bio-mineralization process [4, 26].

In mice, Oc90 is the major constituent protein and accounts for more than 90% of the organic components of otoconia [19, 21]. The protein acts as an essential organizer of the organic matrix during otoconia genesis by recruiting other minor otoconial proteins, such as Otolin-1 [26, 28]. This organic matrix provides a scaffold for efficient and orientated deposition of $CaCO_3$, and thus determines the size and shape of individual crystals [13, 26]. Deletion of *Oc90* results in remarkably reduced bio-mineralization and the formation of a few giant crystals with abnormal morphology in the utricle and saccule of mutant mice [28]. The presence of a few crystals at all in *Oc90* null mice is likely the result of the compensatory deposition of another matrix molecule, SPARC-like protein 1 (aka Sc1) [24].

Nox3, an inner ear-specific superoxide-generating NADPH oxidase [2], is an essential regulatory protein for otoconia development. Mutations in *Nox3* gene not only lead to the absence of otoconia and severe imbalance in the *head-tilt* mice [17, 27], but also remarkably increase the susceptibility to noise-induced hearing loss of mutant mice [12]. The *head-tilt* mice do not generate nystagmus under magnetic vestibular stimulation, presumably due to the absence of otoconia [23]. Inactivation of the partners of Nox3, $p22^{phox}$ and Noxo1, also results in absent otoconia formation and subsequent imbalance in mice [10, 16]. Nox3 constitutively produces a low level of ROS [3], implicating its importance in basic cellular functions and/or survival. However, the exact role of Nox3 in otoconia development remains unclear.

Nox3 is located in the apical (luminal side) cytoplasmic membrane of hair cells [2, 25]. Oc90 is expressed in the non-sensory epithelia in the inner ear [13, 19, 22, 25], but is secreted and abundant in the endolymph [19]. We postulate that Oc90 in the endolymph and Nox3 on the luminal side can influence each other during otoconia development. In order to test this possibility, in this study we generated *Oc90/Nox3* double heterozygous and homozygous mutant mice by crossing the existing *Oc90* null and *head-tilt* mice, a Nox3 functional null strain (herein referred to as *Nox3* null), and performed balance behavioral, electrophysiological, morphological and molecular cellular analyses.

Materials and methods

Animals

Generation of *Oc90* null mice has been previously described [28]. *Nox3* null mice were obtained from the Jackson Laboratory (stock # 002557, Bar Harbor, ME, USA). The *Nox3* mutant strain has an endogenous retroviral insertion in intron 12, resulting in aberrant splicing that renders absent expression of the gene and is therefore functional null [17].

Both *Oc90* and *Nox3* mice have been backcrossed to and maintained in the C57BL/6J (as C57) genetic background. The backcrossed lines were used to generate the *Oc90* heterozygous (*Oc90* het) and *Nox3* heterozygous (*Nox3* het) mice, or crossed to each other to generate double heterozygous (*Oc90/Nox3* D-het) and double homozygous (*Oc90/Nox3* D-null) mice. *Oc90/Nox3* D-null mice were screened by PCR genotyping using the primer sets described in Zhao et al and Flaherty et al [5, 28]. For *Oc90* mutation, the PCR primer sequences were 5′-TCTAACATCCCATTGCCCAGAGGA-3′, 5′-CCAGCCTGACCTGTTCCTTTGTT-3′ and 5′-AATATCACGGGTAGCCAACGCTATGTC-3′. For *Nox3* mutation, the PCR primer sequences were 5’-GTTCTGGAGCACCACCTTGT-3’, 5’-CCCATAGGGAGCCAAGAAAT-3’ and 5’-TGTCAAGCTGACTCCACCAG-3’. All animal procedures were approved by the Institutional Animal Care and Use Committee at the Boys Town National Research Hospital (BTNRH) and/or the University of Nebraska at Lincoln in accordance with federal and international guidelines on the ethical use of animals.

Rotarod test

A four-lane rotarod (Rotamex-5, Columbus Instruments, Columbus, OH, USA) was used in our experiments. Age-matched mice (2~3 months old, 9 to 16 mice for each genotype) were tested for five consecutive days with three trials a day. All tests were carried out within the same time window of the day (between 1 and 4 pm) to control for possible variations introduced by circadian rhythms. Prior to the test each day, a single training session was done during which each mouse was placed on the rotarod at a constant speed (5 rpm) for 60 seconds. Then the mice were tested on the accelerating rod (5-20 rpm over 3 min) for three consecutive sessions, separated by 10-minute resting periods. A laser sensor detected if the animal fell from the rod and the time and speed of rotation at falling were recorded. After the rotation speed reached 20 rpm, animals which remained on the rotarod were allowed to stay on for another 5 min at a constant speed of 20 rpm. The average latency of fall (time the mice remained on the rotating rotarod) was calculated and plotted for each trial and each genotype. One way ANOVA with Bonferroni correction was used to compare differences between groups.

Measurement of vestibular sensory evoked potentials (VsEPs)

Animals were anesthetized by intraperitoneal injection with a mixture of ketamine (180 mg/kg body weight)/xylazine (20 mg/kg body weight). Depth of anesthesia was monitored and maintenance doses of anesthetic were administered as needed during physiological recording. Body core temperature was maintained at 37.0 ± 0.2°C using a homeothermic heating blanket and rectal thermocouple (FHC, Inc., Bowdoin, ME).

VsEPs recording methods were as published previously [6, 7, 20] and are briefly described here. Vestibular stimuli were delivered by securing the head using non-invasive spring clip to a voltage-controlled mechanical shaker. Linear acceleration pulses (17 pulses/s, 2 ms duration) ranged from +6 dB to −18 dB re: 1.0 g/ms (where 1 g = 9.8 m/s^2) adjusted in 3 dB steps were presented along the naso-occipital cranial axis. Needle electrodes were placed posterior to the left pinna and at the ventral neck or hip (inverting and ground electrodes, respectively). Stainless-steel wire was placed subcutaneously at the nuchal crest served as noninverting electrode. Ongoing electroencephalographic activity was amplified (200,000x), filtered (300–3000 Hz, −6 dB amplitude points) and digitized (1024 points, 10 μs/pt). 256 primary responses were averaged and replicated for each VsEP waveform. VsEP intensity series were collected beginning at the maximum stimulus level (i.e., +6 dB re: 1.0g/ms) with and without acoustic masking, then descending in 3 dB steps to −18 dB re: 1.0g/ms. A broad-band forward masker (50–50,000 Hz, 97 dB SPL) was presented during VsEP measurements to verify absence of cochlear responses [8]. The first three positive and negative response peaks were scored for VsEPs. Response peak latencies (P1, N1, P2, measured in milliseconds), peak-to-peak amplitudes (P1-N1 and P2-N1, measured in microvolts) and thresholds (measured in dB re: 1.0 g/ms) were quantified.

Multivariate analysis of variance (MANOVA) with Bonferroni correction was used to compare response peak latencies amplitudes and thresholds of VsEPs between genotypes.

Scanning electron microscopy (SEM)

Animals were anesthetized using ketamine (200 mg/kg) and xylazine (5 mg/kg), followed by decapitation. Whole inner ears were fixed in 3% glutaraldehyde in 0.1 M sodium cacodylate buffer (pH 7.2) containing 3 mM $CaCl_2$ overnight at 4°C. Fine dissection was then performed in artificial endolymph (125 mM KCl, 25 mM $KHCO_3$, 5 mM HEPES, 2 mM $CaCl_2$, 1 mM NaCl) to separate the utricle and saccule. The “roof” of the utricle and saccule was gently removed to expose the otoconia, and otoconia were removed in some samples to expose the sensory epithelia. Tissues were washed three times in artificial endolymph, and post-fixed in 1% osmium tetroxide in 0.1 M sodium cacodylate buffer for 1 h. Samples were then washed three times in artificial endolymph, dehydrated, critical point dried in CO_2, mounted, sputter coated with gold palladium and viewed on a FEI Quanta 200 SEM at 15-20KV.

Phalloidin staining

Mouse inner ears were dissected and fixed in 4% paraformaldehyde for 4 hrs at 4°C. The utricle and saccule were then dissected out of the inner ear in 1X PBS, decalcified in 0.25 M EDTA prepared in 1X PBS for 2 hrs at 4°C, washed three times with 1X PBS, followed by an incubation with a 25 μg/ml FITC-conjugated phalloidin solution (Cat# P5282, Sigma-Aldrich, St. Louis, MO, USA) containing 0.1% Triton X-100 for 1 hr at room temperature in the dark. Unbound conjugated phalloidin was washed off with 1X PBS, and tissues were mounted and viewed using a Zeiss LSM 510 confocal microscope.

Construction of expression vectors

Full-length *Oc90* and *Nox3* transcripts were amplified by RT-PCR of postnatal mouse inner ear tissues and unidirectionally cloned into pTracer-EF/V5-His(C) (*pOc90*) and pcDNA3.1 (*pNox3*). The RT-PCR primers were 5'-ggaattcATGATTATGCTGCTCATGGTCGGT-3' and 5'-gctcgagTTTCCCACCGAGGGGTCTGGCCC-3' for *Oc90*, and 5'-acagaattcATGCAACGCACAGGCTCAAATG-3' and 5'-acactcgagAGTGCATTGACTGTACCC-3' for *Nox3*. Nucleotides in lower cases were non-endogenous sequences to create restriction sites for cloning, and restriction enzymes used were EcoR I (Cat# R0101, NEB, Ipswich, MA) and Xho I (R0146, NEB) for both *Oc90* and *Nox3*. Constructs were confirmed by DNA sequencing and correct protein expression was confirmed by Western blotting.

Cell culture and stable transfection

NIH/3T3 cells were cultured in Dulbecco's Modified Eagle's Medium containing 4.5 g/l glucose, 4 mM L-glutamine, 100 U/ml penicillin and 10% fetal bovine serum. Conventional culture condition was used at 37°C in a humidified incubator supplemented with 5% CO_2. The cells were transfected with *pTracer-Oc90* (*pOc90*) and *pcDNA3.1-Nox3* (*pNox3*), alone or together, and with the empty vector *pcDNA3.1* or *pTracer* using FuGENE® HD (Cat# 4709705001, Roche Applied Science, Indianapolis, IN). Stably transfected clones were selected over a two-week period using 400 μg/ml Zeocin (Cat# R25001, Invitrogen, San Diego, CA) for *pOc90*, or 800 μg/ml G418 (Cat# 11811023, Invitrogen, San Diego, CA) for *pNox3*. Selected clones were then expanded and analyzed for calcification potential as described below.

Induction of extracellular matrix (ECM) calcification

To induce ECM mineralization, stable NIH/3T3 clones expressing *pOc90, pNox3, pOc90+pNox3, pcDNA3.1* (empty vector) were treated with 0.5 mM Ca^{2+} ($CaCl_2$) and 2 mM Pi (Na_2HPO_4) in growth media to provide a source of inorganic components for mineralization [24, 26]. Phosphate, instead of carbonate, was used so as not to alter the optimal pH and CO_2 content. On the sixth day, cells were fixed with 4% paraformaldehyde, and stained with Alizarin Red S (ARS) (Cat# A5533, Sigma-Aldrich). Calcification nodules and total cells were photographed and counted for each 20x view field under an inverted microscope (approximately 1.2 mm^2); averaged ratios of nodules/total cells were compared among transfectants and the empty vector using one way ANOVA with Bonferroni correction.

Data Analysis

Reported data represent the mean values ± standard deviation. Statistical significance was determined by ANOVA or MANOVA with Bonferroni correction, as described at the end of each procedure. Significance was set at the level of $p<0.05$. *P* values are expressed as * or $^{\$}$ $p<0.05$, ** $p<0.01$, and ***, $^{\#\#\#}$ or $^{\$\$\$}$ $p<0.001$.

Results

Oc90/Nox3 double mutant mice had severe balance deficits

The balance function of *Oc90* and *Nox3* single and double mutants, along with age-matched wild-type (WT), was examined by rotarod tests. While deficits in other systems (such as the central nervous system and neuromuscular system) can also influence rotarod performance, only inner ear deficits are known to exist in these two lines of mutant mice as *Oc90* and *Nox3* genes are reported to be primarily expressed in the inner ear [2, 6, 17, 27, 28]. All double null and single null mice stayed on the rotarod for a significantly shorter time than WT mice in all trials, with *Oc90/Nox3* double null and *Nox3* single null mice as the worst performers (Fig. 1, $p<0.01$ between double mutants and WT, as well as between single mutants and WT). The order of best to worst performers was WT (n=14), *Oc90* null (n=16), *Oc90/Nox3* D-het (n=12), *Nox3* single null (n=9) and *Oc90/Nox3* D-null (n=11). Single heterozygous mice have normal balance function and normal inner ear histology [27, 28]. Surprisingly, double heterozygous mice could stay on the rotarod for significantly less time than the WT mice ($p<0.01$). The difference between double null and double heterozygous mice was also significant ($p<0.05$ except Day1). Such poor rotarod performance of *Oc90/Nox3* double mutants is indicative of the severe balance deficits which caused them to fall from the rod much easier than the WT mice.

Interestingly, the difference between the mutants and WT mice became even greater with each subsequent trial, as the WT mice improved their performance much more over time. Double null and *Nox3* single null mice did not improve their performance over time. The slope of improvement ranked the same order as their balance functions stated above, with a nearly four-fold increase in latencies on the rotarod on day 5 as compared with day 1 for WT mice ($p<0.001$).

Measurement of VsEPs confirmed the vestibular dysfunction in *Oc90/Nox3* double mutants

The vestibular function of *Oc90/Nox3* double mutant mice was further evaluated by measuring the vestibular evoked potentials (VsEPs). As shown in Table 1, *Oc90/Nox3* D-het mice (n=8) showed significantly elevated VsEP thresholds, longer latencies, and smaller peak-to-peak amplitudes than those of age-matched C57 mice (n=4, $p<0.05$ vs. C57). The VsEP responses in *Oc90/Nox3* D-nulls (n=6) were completely absent.

Linear VsEPs are compound action potentials generated by the vestibular nerve and its central relays in response to linear acceleration. They depend critically on the utricle and saccule, and provide a direct measure of the functional status of those two organs [6, 9]. Thus, the significantly changed VsEPs recordings reflect the impaired gravity receptor function in *Oc90/Nox3* D-het and D-null mice.

Oc90/Nox3 D-het and D-null mice had abnormal and absent otoconia, respectively

As with *Nox3* null mice, otoconia were completely absent in the utricle and saccule in *Oc90/Nox3* D-null mice [Fig. 2C, all mice were postnatal day 14 (P14)], which may explain their extremely poor rotarod performance shown in Fig. 1. While the D-het mice had otoconia, the crystal morphology was abnormal as shown by scanning electron microscopy in Fig. 2.

In WT mice, the crystals had barrel-shaped bodies and tri-planar facets at each end, and had smooth surfaces (Fig. 2A). In comparison, most of the otoconia in *Oc90/Nox3* D-het mice had fissured surface and irregular shape, and some were fused (Fig. 2B). The percentage of otoconia with rugged surface was much higher in the D-het mice than that in the WT mice (92.9% vs. 3.3%, n=5, $p<0.001$, Fig. 2D).

Some hair bundles in *Oc90/Nox3* D-null mice went through accelerated degeneration

Whole-mount phalloidin staining was performed to examine the gross morphology of hair bundles in the vestibule of WT and mutant mice. Phalloidin staining of F-actin in hair bundles showed that *Oc90/Nox3* D-null mice had some loss of hair bundles in the utricle and saccule at 3 months (3M) of age (Fig. 3B vs. 3A; the saccule is shown). At this age, there were approximately 2.8 bundles per $100\mu m^2$ in the WT saccule, whereas D-null only had 1.8 bundles per $100\mu m^2$ (n=6, $p<0.001$). No gross abnormality was apparent in hair bundles in D-null mice at perinatal ages (data not shown), suggesting that the bundle loss occurred at later ages and likely arose from accelerated degeneration. D-het mice had normal-appearing hair bundles similar to those in WT mice (data not shown).

Synergy between Oc90 and Nox3 in facilitating extracellular matrix (ECM) calcification

Our previous studies have shown that the presence of Oc90 can augment ECM calcification in cell culture [24, 26]. In this study, the pro-calcification efficiency of Oc90 and Nox3 in cultured cells was compared by a similar induction system. NIH/3T3 cells stably transfected with the empty vector, *pOc90* and/or *pNox3* were cultured for 5 days in media supplemented with 0.5 mM Ca^{2+} and 2 mM Pi as calcification-inducing condition. Inorganic calcium deposits were then visualized with Alizarin Red S (ARS) staining and imaged on the 6^{th} day. Averaged percentages of cells covered with calcified nodules over total cells in each sample were calculated and plotted. As shown in Fig. 4, Nox3 slightly but significantly increased calcification when compared with cells transfected with the empty vector (** $p< 0.01$), and Oc90 had a much greater effect than Nox3 (### $p< 0.001$, n=9 in each group). Co-transfection of *Oc90* and *Nox3* drastically increased matrix calcification under the same inducing conditions, when compared with the empty vector, Oc90 or Nox3 single transfection ($p= 4.75 \times 10^{-13}$, 5.96×10^{-13} and 1.23×10^{-7}, respectively, n=9 each). These data demonstrate the functional synergy between Oc90 and Nox3 in promoting matrix calcification *in vitro*.

Discussion

Although there is the general notion that otoconia development is a sophisticated biomineralization process and requires the coordinated participation of numerous proteins [14, 15, 25], it is unknown whether and how the constituent and regulatory proteins work together for optimal crystal formation. Our current investigation of the *Oc90/Nox3* double mutant mice shows that Oc90, the major constituent otoconin, and Nox3, a regulatory protein, functionally cooperate to ensure the correct formation of otoconia as well as normal balance function.

Given the absent otoconia in *Nox3* single null mice [17], and a few giant otoconia in *Oc90* null mice [28], it is not surprising that *Oc90/Nox3* D-null mice do not have any otoconia or VsEPs response at all (Fig. 2 and Table 1). It is unanticipated, however, that *Oc90/Nox3* double heterozygous mice exhibit deficits in otoconia and balance behaviors, when both *Oc90* and *Nox3* single heterozygous mice are normal in these functions [17, 27]. Such deficits are even more severe in D-null mice (Fig. 1, Table 1). Morphological examination revealed compromised hair bundle maintenance as well in adult *Oc90/Nox3* D-null mice (Fig. 3), suggesting deficits in hair cell functions. The functional synergy between Oc90 and Nox3 is further confirmed in analysis of extracellular matrix calcification (Fig. 4). It is possible that there is less effective cooperation of Oc90 and Nox3 in the *Oc90/Nox3* double heterozygous mice, severe enough to cause functional loss but not gross morphological abnormality of hair bundles.

Because otoconia are composed of numerous minute crystallites that are each embedded in organic matrix [28], the fissured surface in D-het mice (Fig. 2) might be attributed to insufficient and/or inappropriate deposition of organic components. Nox3 may oxidize the thiol groups in Oc90, generating Oc90 dimers or even multimers via formation of disulfide bonds, thus converting Oc90 from soluble (in endolymph) to matrix form to serve as a scaffold for $CaCO_3$ crystal seeds to deposit and grow. In addition, superoxide generated by Nox3 may elevate local pH by reacting with protons (the endolymph has a pH of 7.4) as proposed by [16], and thus help maintain the transmembrane potential and prevent the fluid from becoming too acidic from CO_2 generated by cellular metabolism. The elevated pH is optimal for otoconia formation and maintenance, as well as for mechanotransduction by hair cells.

Conclusion:

Our data show that Oc90 and Nox3 are not only coordinately involved in otoconia morphogenesis, but also functionally interlinked to optimize hair bundle maintenance. Taken together with other published data, we derive the overall impression that optimal otoconia crystallization arises from interactions of multiple proteins, perhaps in sequential steps. Further research is needed to uncover the molecular details about how these proteins work together in those processes.

Funding

The work was supported in part by grants from the National Institutes of Health (DC008603, DC008603-S1 and DC014748 to Y.W.L.).

Reference List

[1]. Anniko M, Wenngren BI and Wroblewski R, Aberrant elemental composition of otoconia in the dancer mouse mutant with a semidominant gene causing a morphogenetic type of inner ear defect, Acta Otolaryngol 106 (1988), 208–212. [PubMed: 3176966]

[2]. Banfi B, Malgrange B, Knisz J, Steger K, Dubois-Dauphin M and Krause KH, NOX3, a superoxide-generating NADPH oxidase of the inner ear, J. Biol. Chem 279 (2004), 46065–46072. [PubMed: 15326186]

[3]. Bedard K and Krause KH, The NOX family of ROS-generating NADPH oxidases: physiology and pathophysiology, Physiol Rev 87 (2007), 245–313. [PubMed: 17237347]

[4]. Deans MR, Peterson JM and Wong GW, Mammalian Otolin: a multimeric glycoprotein specific to the inner ear that interacts with otoconial matrix protein Otoconin-90 and Cerebellin-1, PLoS. ONE 5 (2010), e12765. [PubMed: 20856818]

[5]. Flaherty JP, Fairfield HE, Spruce CA, McCarty CM and Bergstrom DE, Molecular characterization of an allelic series of mutations in the mouse Nox3 gene, Mamm. Genome 22 (2011), 156–169. [PubMed: 21161235]

[6]. Jones SM, Erway LC, Bergstrom RA, Schimenti JC and Jones TA, Vestibular responses to linear acceleration are absent in otoconia-deficient C57BL/6JEi-het mice, Hear. Res 135 (1999), 56–60. [PubMed: 10491954]

[7]. Jones SM, Erway LC, Johnson KR, Yu H and Jones TA, Gravity receptor function in mice with graded otoconial deficiencies, Hear. Res 191 (2004), 34–40. [PubMed: 15109702]

[8]. Jones TA and Jones SM, Short latency compound action potentials from mammalian gravity receptor organs, Hear. Res 136 (1999), 75–85. [PubMed: 10511626]

[9]. Jones TA and Jones SM, Vestibular evoked potentials., in: Auditory Evoked Potentials: Basic Principles and Clinical Applications., Burkard RFDM;Eggermont JJ ed., Lippincott Williams & Wilkins, Baltimore, MD, 2007.

[10]. Kiss PJ, Knisz J, Zhang Y, Baltrusaitis J, Sigmund CD, Thalmann R, Smith RJ, Verpy E and Banfi B, Inactivation of NADPH oxidase organizer 1 Results in Severe Imbalance, Curr. Biol 16 (2006), 208–213. [PubMed: 16431374]

[11]. Kozel PJ, Friedman RA, Erway LC, Yamoah EN, Liu LH, Riddle T, Duffy JJ, Doetschman T, Miller ML, Cardell EL and Shull GE, Balance and hearing deficits in mice with a null mutation in the gene encoding plasma membrane Ca2+-ATPase isoform 2, J. Biol. Chem 273 (1998), 18693–18696. [PubMed: 9668038]

[12]. Lavinsky J, Crow AL, Pan C, Wang J, Aaron KA, Ho MK, Li Q, Salehide P, Myint A, Monges-Hernadez M, Eskin E, Allayee H, Lusis AJ and Friedman RA, Genome-wide association study identifies nox3 as a critical gene for susceptibility to noise-induced hearing loss, PLoS. Genet 11 (2015), e1005094. [PubMed: 25880434]

[13]. Lu W, Zhou D, Freeman JJ, Thalmann I, Ornitz DM and Thalmann R, In vitro effects of recombinant otoconin 90 upon calcite crystal growth. Significance of tertiary structure, Hear. Res 268 (2010), 172–183. [PubMed: 20595020]

[14]. Lundberg YW and Xu Y, Proteins Involved in Otoconia Formation and Maintenance, in: Otolaryngology, Gendeh BS ed., InTech, 2012, pp. 3–22.

[15]. Lundberg YW, Xu Y, Thiessen KD and Kramer KL, Mechanisms of otoconia and otolith development, Dev. Dyn 244 (2015), 239–253. [PubMed: 25255879]

[16]. Nakano Y, Longo-Guess CM, Bergstrom DE, Nauseef WM, Jones SM and Banfi B, Mutation of the Cyba gene encoding p22phox causes vestibular and immune defects in mice, J. Clin. Invest 118 (2008), 1176–1185. [PubMed: 18292807]

[17]. Paffenholz R, Bergstrom RA, Pasutto F, Wabnitz P, Munroe RJ, Jagla W, Heinzmann U, Marquardt A, Bareiss A, Laufs J, Russ A, Stumm G, Schimenti JC and Bergstrom DE, Vestibular defects in head-tilt mice result from mutations in Nox3, encoding an NADPH oxidase, Genes Dev 18 (2004), 486–491. [PubMed: 15014044]

[18]. Simmler MC, Cohen-Salmon M, El-Amraoui A, Guillaud L, Benichou JC, Petit C and Panthier JJ, Targeted disruption of otog results in deafness and severe imbalance, Nat. Genet 24 (2000), 139–143. [PubMed: 10655058]

[19]. Verpy E, Leibovici M and Petit C, Characterization of otoconin-95, the major protein of murine otoconia, provides insights into the formation of these inner ear biominerals, Proc. Natl. Acad. Sci. U. S. A 96 (1999), 529–534. [PubMed: 9892667]

[20]. Vijayakumar S, Depreux FF, Jodelka FM, Lentz JJ, Rigo F, Jones TA and Hastings ML, Rescue of peripheral vestibular function in Usher syndrome mice using a splice-switching antisense oligonucleotide, Hum. Mol. Genet 26 (2017), 3482–3494. [PubMed: 28633508]

[21]. Wang Y, Kowalski PE, Thalmann I, Ornitz DM, Mager DL and Thalmann R, Otoconin-90, the mammalian otoconial matrix protein, contains two domains of homology to secretory phospholipase A2, Proc. Natl. Acad. Sci. U. S. A 95 (1998), 15345–15350. [PubMed: 9860971]

[22]. Wang Y, Thalmann I, Thalmann R and Ornitz DM, Mapping the mouse otoconin-90 (Oc90) gene to chromosome 15, Genomics 58 (1999), 214–215. [PubMed: 10366455]

[23]. Ward BK, Lee YH, Roberts DC, Naylor E, Migliaccio AA and Della Santina CC, Mouse Magnetic-field Nystagmus in Strong Static Magnetic Fields Is Dependent on the Presence of Nox3, Otol Neurotol 39 (2018), e1150–e1159. [PubMed: 30444848]

[24]. Xu Y, Zhang H, Yang H, X Z., Lovas S and Lundberg YW, Expression, functional and structural analysis of proteins critical for otoconia development, Dev. Dyn 239 (2010), 2659–2673. [PubMed: 20803598]

[25]. Xu Y, Zhang Y and Lundberg YW, Spatiotemporal differences in otoconial gene expression, Genesis 54 (2016), 613–625. [PubMed: 27792272]

[26]. Yang H, Zhao X, Xu Y, Wang L, He Q and Lundberg YW, Matrix recruitment and calcium sequestration for spatial specific otoconia development, PLoS. ONE 6 (2011), e20498. [PubMed: 21655225]

[27]. Zhao X, Jones SM, Yamoah EN and Lundberg YW, Otoconin-90 deletion leads to imbalance but normal hearing: a comparison with other otoconia mutants, Neuroscience 153 (2008), 289–299. [PubMed: 18355969]

[28]. Zhao X, Yang H, Yamoah EN and Lundberg YW, Gene targeting reveals the role of Oc90 as the essential organizer of the otoconial organic matrix, Dev. Biol 304 (2007), 508–524. [PubMed: 17300776]

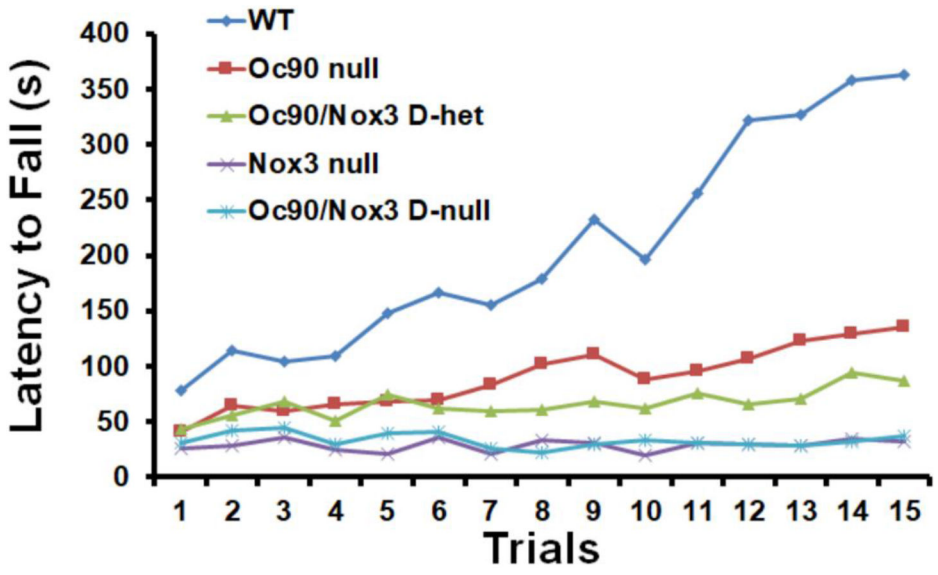

Fig. 1. Severe balance deficits of *Oc90/Nox3* double mutant mice by rotarod tests (all mice were 1.5 months old).

Oc90/Nox3 D-het mice (n=12) could stay on the accelerating rotarod for a significantly shorter time than WT mice (n=14, $p<0.001$). The latencies of *Oc90/Nox3* D-null mice (n=11) were even shorter ($p<0.01$ vs. D-hets, $p<0.05$ vs. *Oc90* null mice, and $p<0.001$ vs. WT) and were similar to that of *Nox3* null mice (n=9).

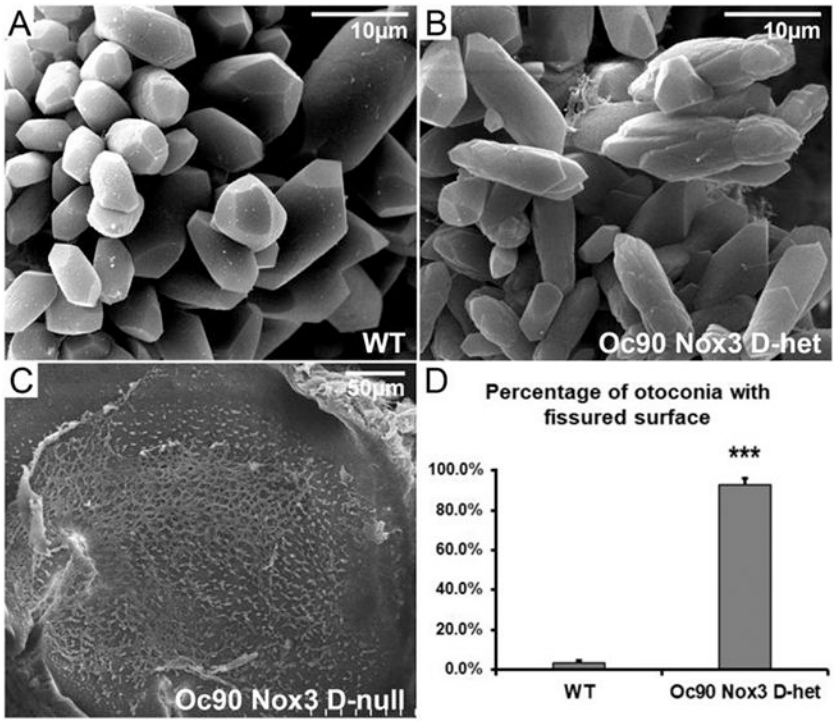

Fig. 2. Abnormal otoconia morphology in the *Oc90/Nox3* double heterozygous mice by scanning electron microscopy.

(A) Otoconia crystals in WT mice have normal barrel-shaped bodies and tri-planar facets at the ends with smooth surfaces. **(B)** Crystals in *Oc90/Nox3* D-het mice have irregular shapes and fissured surfaces. **(C)** No otoconial crystal is found in *Oc90/Nox3* D-null mice. (D) The percentage of otoconia with rugged surface is much higher in the D-het mice than that in the WT mice (92.9% vs. 3.3%, n=5, *** indicates $p<0.001$). P14 utricles are shown.

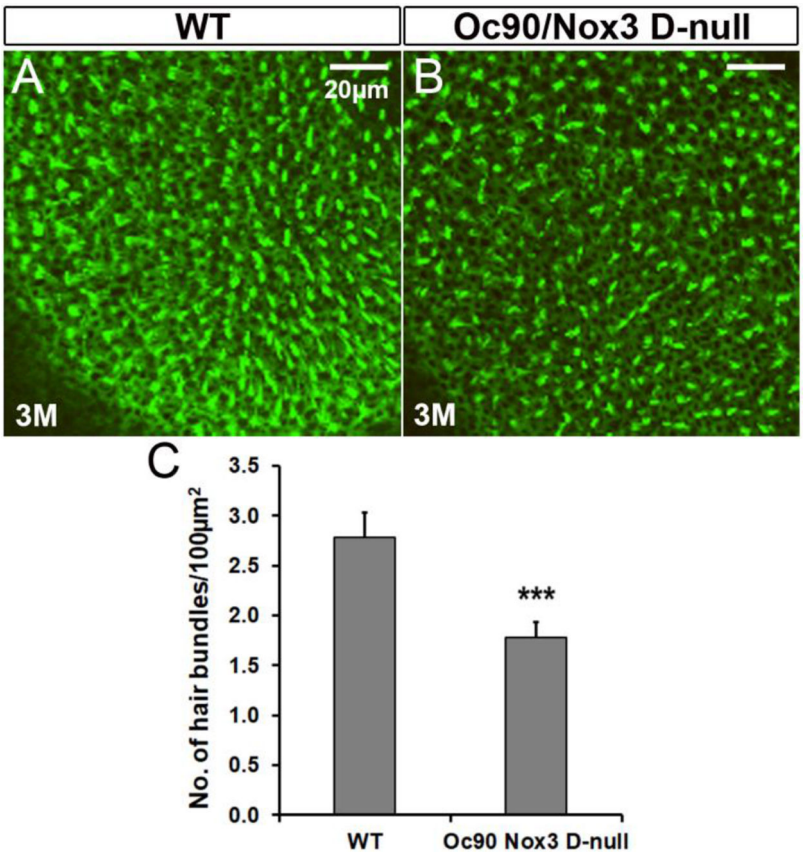

Fig. 3. Accelerated hair bundle degeneration in *Oc90/Nox3* D-mutant mice as shown by phalloidin staining.

(B) Loss of hair bundles in *Oc90/Nox3* D-null mice in comparison with age-matched WT mice (**A**) (saccules are shown). **(C)**. Numbers of hair bundles per 100μm^2 in WT and D-null saccules (n=6, *** indicates p<0.001). Scale bars: **A & B,** 20μm. 3M, aged 3 months old.

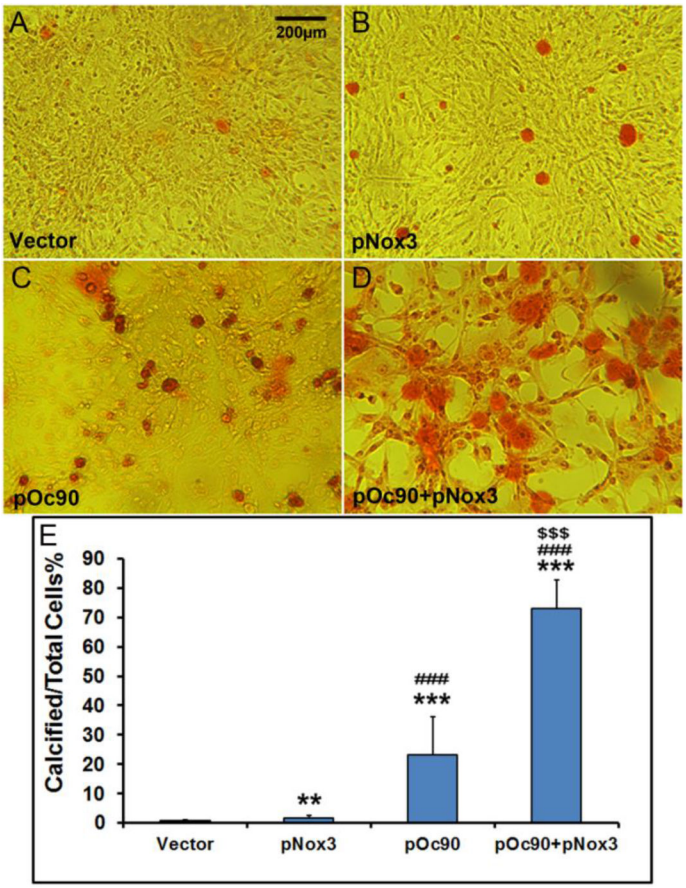

Fig. 4. Synergy between Oc90 and Nox3 in promoting extracellular matrix calcification.

NIH/3T3 cells stably transfected with empty vector **(A)**, *pNox3* **(B)**, *pOc90* **(C)** and *pOc90+pNox3* **(D)** were cultured in media supplied with 0.5mM Ca^{2+} and 2mM Pi for 5 days. Extracellular matrix calcium deposits were visualized with Alizarin Red S staining on the 6th day, and averaged percentages of cells covered with calcified nodules over total cells were calculated and plotted **(E)**. ** and *** indicates p<0.01 and 0.001 vs. empty vector, respectively; ### indicates p<0.001 vs. *pNox3*; $$$ indicates p<0.001 vs. *pOc90*, n=9 each.

Table 1.

Oc90/Nox3 double null mice had absent VsEPs. Double heterozygotes mice had significantly elevated VsEP thresholds, longer latencies, and smaller amplitudes when compared with age-matched C57 mice (1.5 months old). All measurements below for the D-hets showed $p<0.05$ when compared with those for C57 mice. NR = no response.

Group	Threshold (dB re: 1g/ms)	P1 (ms)	P2 (ms)	P1-N1(μV)	P2-N2(μV)
C57 (n=4)	−9.70 ± 2.11	1.28 ± 0.05	2.01 ± 0.12	0.66 ± 0.11	0.48 ± 0.18
Oc90/Nox3 D-het (n=8)	−3.0 ± 1.64	1.44 ± 0.15	2.34 ± 0.17	0.40 ± 0.16	0.38 ± 0.17
Oc90/Nox3 D-null (n=6)	NR	NR	NR	NR	NR